CLUTTER MAPPING FOR AIRBORNE PULSE DOPPLER RADAR

C.M. Alabaster*, E.J. Hughes*

*Cranfield University, DCMT Shrivenham, OXON, SN6 8LA, UK. Email c.m.alabaster@cranfield.ac.uk

Keywords: Medium PRF, radar, clutter, detectability.

Abstract

This paper presents a quick and simple method to model the surface clutter map of an airborne radar operating in a medium pulse repetition frequency (PRF) mode and in a look-down scenario. The basic model derives a clutter map in the range/velocity detection space of the radar specific to each PRF used within the radar schedule. Additional functionality may be introduced which permits regions of differing clutter statistics to be defined and which computes target detectability over the range/velocity detection space of the radar. The models described here have been used successfully in a variety of research tasks to optimise PRF selection and weighting functions of a phased array antenna.

1 Introduction

In many pulse Doppler radar applications it is necessary to determine the clutter power across the range/velocity detection space of the radar. Such a facility enables the designer to judge in which regions target detection may be clutter limited as opposed to noise limited and the smallest target radar cross section (RCS) which may be detectable in any given scenario. For airborne radars the situation is complicated since side lobe clutter (SLC) will occupy a Doppler band, Δf_d given by:

$$\Delta f_d = \pm \frac{2.V}{\lambda} \qquad (1)$$

where V is the ground speed of the aircraft platform, λ is the transmitted wavelength and the ± arises because the forward facing antenna mainbeam and sidelobes perceive the ground as a closing target and the rearward facing sidelobes and backlobe perceive the ground as a receding target. Airborne pulse Doppler radars typically operate in a medium pulse repetition frequency (PRF) mode in which both range and Doppler are ambiguous. Range and Doppler ambiguities are resolved by cycling the operation of the radar over a number of coherent processing intervals (CPI) each at a different PRF within the beam dwell time. Typically, 6 to 9 PRFs may be used. Medium PRF and, in particular, PRF selection, is described in our previous papers [1]-[3][8]. The range extent of surface clutter and its Doppler extent typically occupy more than one unambiguous interval in range and velocity, respectively. As a result, clutter is repeated at multiples of the pulse repetition interval (PRI =1/PRF) in the time (i.e. range) domain and at multiples of the PRF in the Doppler (i.e. velocity) domain. In airborne systems it is also common place to perform platform motion compensation (PMC) in order to reference all velocities with respect to the ground. This requires that a Doppler offset be applied to all data commensurate with the component of the forward velocity of the aircraft resolved along the main beam boresight. In this way, main beam clutter (MBC) will be centred at zero Doppler and repeated at multiples of the PRF. The clutter power in the range/velocity detection space of the radar depends on the platform velocity and altitude, grazing angle, surface backscatter coefficient, antenna radiation diagram and scan angles and, crucially, PRF. It may be further modified by signal processing gains and losses and decorrelation due to clutter motion. Accurate mapping of the clutter in range and velocity is important in the selection of precise values of PRF within a schedule and the optimum antenna radiation diagrams. This enables the signal to clutter ratio (SCR) to be derived and target detectability to be assessed.

This paper describes a method of mapping clutter in the range/velocity detection space of an airborne pulse Doppler radar operating in a medium (or for that matter a high or low) PRF mode. The next section of this paper describes the model and the formation of clutter maps. The following section describes additional functionality which can be introduced into the basic model such as the adoption of a curved earth geometry, the introduction of zones of differing clutter statistics and accounting for the decorrelation arising from internal clutter motion (ICM) and how such models may be used to assess radar detection performance. The model is easy to implement and has been used and refined on several research projects conducted by the authors in recent years.

2 Basic Model

In the first case it is advisable to produce an *ideal* clutter map, which is a plot of the returning clutter power over the range and velocity detection space of the radar. The ideal clutter map is independent of the range and velocity resolutions of the radar and of its PRFs. Since the clutter data must be quantized in discrete range and velocity intervals, it is initially necessary to select range and velocity cells which are marginally finer than those of the radar under consideration.
Clutter is mapped by considering the surface under the radar to be marked out by a grid along orthogonal x and y coordinates centred at 0,0 directly under the radar. The model steps through increments in the x and y coordinates out to the

maximum range of interest. At each location the model computes the slant and ground ranges and the resolved Doppler shift along the line of sight to the radar together with the grazing angle using simple trigonometrical identities.

An important aspect of the clutter mapping process is the resolution of the increments along the *x/y* coordinate system. At each location, the clutter backscatter coefficient is derived and clutter radar cross section (RCS_C) is computed on the basis of a clutter area equal to the square of the *x/y* resolution. Ideally, the *x/y* resolution should be finer than the radar range resolution since otherwise there will be large clutter patches appearing in some resolution cells and nothing in neighbouring cells. However, *very* fine *x/y* resolution is unnecessary and increases the computational time. A reasonable compromise is to set the *x/y* resolution to marginally less than the radar range resolution. The clutter backscatter coefficient (BSC) is a function of the grazing angle, θ_g, which is computed for each point in the clutter modelling process. A suitable function relating BSC to grazing angle may be defined as:

$$BSC = \sigma_0 \sin(\theta_g) + \sigma_{0V}\ w.\exp\left(\frac{-(90-\theta_g)}{\theta}\right) \qquad (2)$$

in which $\theta = \dfrac{-20}{\log_e(\sin 70^0 / A)}$ and $A = \dfrac{\sigma_{0V}}{\sigma_0}$

w is a statistical parameter defined by the probability density function (PDF) appropriate to the clutter, σ_{0V} defines the BSC at normal incidence and σ_0 defines the BSC at a mid grazing angle. The function defined by (2) provides a good fit to measured data [5],[6]. Clutter was generated using a variable with a Weibull power distribution given by:

$$w = B\sqrt[C]{-\ln(U)} \qquad (3)$$

where U is a uniformly distributed random number in the range [0,1], B is the distribution spread and C is the shape parameter. For land clutter typical values are $B = C = 1$ whereas for sea clutter $B = 0.1$ and $C = 0.65$ are typical. Should the statistical variation not be required, one may use the mean value of the clutter distribution. The mean of (3) is given by:

$$mean = B.\Gamma\left(\frac{(C+1)}{C}\right) \qquad (4)$$

where Γ denotes the gamma function.

For land clutter $B = C = 1$ and therefore the *mean* = w = 1. The dependence of BSC on grazing angle is depicted in Figure 1 in which w = 1 and in which the solid line refers to the case of σ_0 = -13 dBm^2 and σ_{0V} = -5 dBm^2 and the dashed line refers to the case of σ_0 = -22 dBm^2 and σ_{0V} = -15 dBm^2. The higher values have been used here.
Finally, the clutter radar cross section is derived from:

$$RCS_C = \text{BSC} \times (x/y\ resolution)^2 \qquad (5)$$

The power of the clutter returns is then calculated using the following form of the radar range equation in which the RCS_C is cascaded with the transmitting and receiving antenna gains along the line of sight to the radar by reference to the appropriate antenna radiation pattern data.

$$clutter\ power = \frac{P_T.G_T.G_R.\lambda^2.RCS_C}{64.\pi^3.R_S^4} \qquad (6)$$

where P_T = peak transmitted power
G_T = transmitting antenna gain
G_R = receiving antenna gain
R_S = slant range

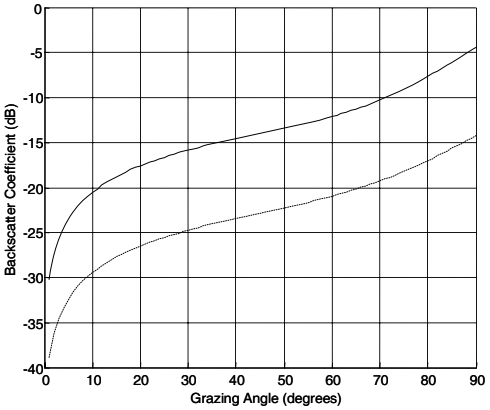

Figure 1: Surface Clutter Back Scatter Coefficient vs. Grazing Angle for Two Different Scattering Conditions

The solution to (6) requires that full knowledge of the transmitting and receiving antenna gains, G_T and G_R, at any desired azimuth and elevation steering angles are available. This may be derived from a model of the antenna and is considered outside the scope of this paper.

A display of the returning clutter power against range and velocity may be derived. An example is given in Figure . From Figure one may observe the spectral band of clutter, the stripes corresponding to SLC and a region of intense clutter centred at around velocity cell 2800 and range cell 100 which is the main beam footprint on the ground (MBC). The next stage of the computation entails the production of a *folded* clutter map in which the clutter amplitude from the full detection space of the radar is folded into one ambiguous range and Doppler interval, both of which are PRF dependent. Furthermore, it is now desirable to plot folded clutter map data within range and velocity increments corresponding to the radar range and velocity resolution, both of which may also be PRF dependent. Thus a folded clutter map always has a number of Doppler cells equal to the FFT size but a variable number of range cells which is equal to the number of range cells in one PRI. For radars operating over multiple PRFs, a folded clutter map unique to each PRF must be derived. However, the data of the ideal clutter map is not dependent on PRF and may be used as the basis for each folded clutter map. Thus a repeat of the lengthy clutter simulation is not required for each PRF.

The clutter power calculated from the ideal clutter map is read out from each pixel in the image and assigned to its

appropriate range and velocity cell. For range, the operation runs as:

$$\text{range cell} = \frac{R}{R_{res}} \text{modulo} \left(\frac{R_{mu}}{R_{res}} \right) \quad (7)$$

where R = range
R_{res} = range resolution,
R_{mu} = maximum unambiguous range
and $(R_{mu} = c/2.f_r)$ where c = speed of propagation, f_r = PRF

The quantity $\left(\frac{R_{mu}}{R_{res}} \right)$ represents the number of range cells in one receiving period.

Similarly, for Doppler, the Doppler cell is defined as:

$$\text{Doppler cell} = \frac{f_d}{f_{dres}} \text{modulo} \left(\frac{f_r}{f_{dres}} \right) \quad (8)$$

where f_d = Doppler frequency
f_{dres} = Doppler resolution $(f_{dres} = f_r / FFT\ size)$

The quantity $\left(\frac{f_r}{f_{dres}} = FFT\ size \right)$ represents the number of Doppler cells within one PRF interval. Doppler and Doppler cells can then be readily translated to the velocity domain, V, by the relationship:

$$V = \frac{\lambda . f_d}{2} \quad (9)$$

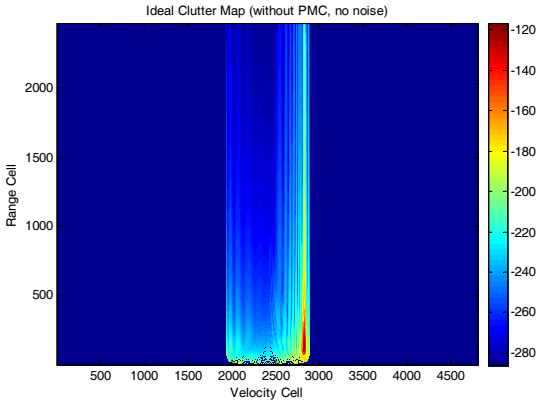

Figure 2: Ideal Clutter Map

A constant fixed noise power level of $k.T_0.B_n.F$ is added in to every cell of the folded clutter map, in which k is Boltzmann's constant = 1.38×10^{-23}, T_0 is a standard temperature of 290K, B_n is the noise bandwidth = (transmitted pulse width)$^{-1}$ and F is the noise figure. Clutter amplitudes are read out of the ideal clutter map, range and Doppler gated and added into the appropriate cells of the folded clutter map on top of the noise power and any previously calculated clutter signals. Clutter power is also subject to a processing gain of the FFT size but then to subsequent signal processing, transmit and receive losses, atmospheric attenuation and additional losses due to the ICM effects (see next section). PMC is applied by pre-calculating the Doppler gate of the centre of the main beam and applying this as an offset to the Doppler gated clutter. The total clutter and noise power is then stored in a two-dimensional matrix (range cell vs. Doppler cell) and displayed on a folded clutter map. An example of a folded clutter map is given in Figure 3. The final stage entails the production of the *unfolded* clutter map. The folded clutter map may be unfolded to cover the complete range/velocity detection space specified by the radar model by tiling the folded clutter map as many times as necessary. An example unfolded clutter map is given in Figure 4.

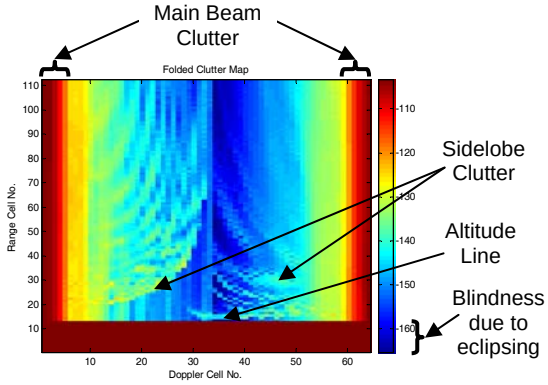

Figure 3: Folded Clutter Map

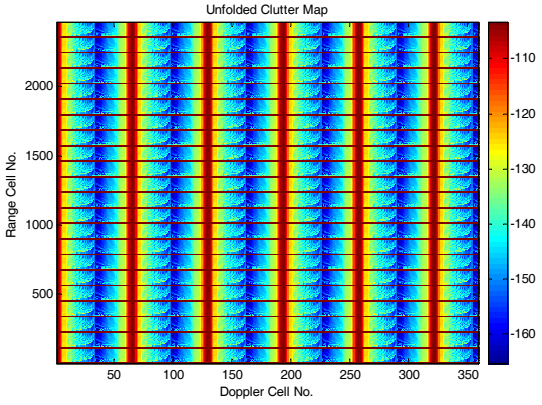

Figure 4: Unfolded Clutter Map

3 Additional Functionality

Having derived (unfolded) clutter maps for each PRF, scan angle and platform scenario it is now possible to consider several embellishments to the basic modelling procedure. It is also appropriate to consider how such maps may be utilised for the assessment of system detection performance.

3.1 Curved Earth Geometry

When considering a curved earth geometry, the slant range increases and the grazing angle reduces compared with their flat earth counterparts. The grazing angle adjusted for the curved earth geometry is given by:

$$\theta_g^{/} = \sin^{-1}\left(\frac{(r_e+h)^2 - r_e^2 - R_S^2}{2.R_S.r_e}\right) \qquad (10)$$

where r_e = the earth radius.

In truth, the allowance for a curved earth has minimal effect on the clutter maps and target detectability.

3.2 Internal Clutter Motion (ICM)

Internal clutter motion (ICM) may be included within the clutter model, leading to a small broadening of the clutter region. The ICM is modelled as a spread of velocities which have a Gaussian density function [6], which leads in practice to phase and amplitude modulation of the received pulse train. The probability density distribution of the velocity modulation, *p(v)*, can be described as in (11):

$$p(v) = \frac{1}{\sigma_{cv}\sqrt{2\pi}}\exp\left(\frac{-v^2}{2\sigma_{cv}^2}\right) \qquad (11)$$

where v is velocity in m/s and σ_{cv} is the standard deviation of the clutter internal motion in m/s. The relative power in each velocity cell may be calculated by integrating (11) over each cell interval, with the 0m/s cell being defined as having limits of $\pm V_{res}/2$, where V_{res} is the velocity resolution of the current PRF. (12) details the integration process for each cell of index i, with i = 0 indicating the central cell, and $\pm i$ stepping through the neighbouring cells (i is an integer), resulting in the power contribution in each velocity cell, P_i.

$$P_i = \int_{i-V_{res}/2}^{i+V_{res}/2} p(v)dv \qquad (12)$$

A clutter standard deviation of 1.5m/s appears to be appropriate for the deviation expected from rain and chaff [7 - table 15.1]. With a 1.5m/s standard deviation and Gaussian profile, the central velocity cell retains approximately 38% of the original power for a typical schedule (7ms CPI), with the remaining power spread over the close adjacent velocity cells. A 1m/s standard deviation leads to the central velocity cell retaining approximately 56% of the power and provides a match to the upper-end of anticipated heavy sea clutter. A 0.2m/s standard deviation would be appropriate for agricultural land clutter.

3.3 Zones of Differing Clutter Statistics

Regions of differing clutter statistics may be defined by a variation in the clutter parameters (A, B, C, w, σ_{0V} , σ_0 or θ – equations (2) to (4)) over ranges of the x and y coordinates, as required. This has been done in order to define parameters appropriate to sea clutter to one side (negative x) and land clutter on the other side (positive x) of an aircraft's flight path [1]. The simple Cartesian coordinate system of spatial sampling used in this model makes this type of clutter zoning very easy to implement.

3.4 Assessment of Target Detectability

Target detectability over the full range/Doppler detection space of interest is conveniently represented by a *detectability map* [1],[4]. The probability of detection of a discrete target at any range/Doppler cell of interest depends on the number of PRFs in which the range/Doppler cell is not blind (either due to eclipsing or MBC rejection) and the probability of detection in each PRF, as determined by the signal to noise plus clutter ratio (SNCR) of the cell. In generating a detectability map the unfolded clutter maps of all PRFs in the schedule need to be overlaid and read at a common resolution which can be no finer than the coarsest resolution of any of the unfolded clutter maps. The clutter amplitudes at each range/velocity cell need to be assessed in order to judge the necessary target RCS required to exceed the noise plus clutter with the required SNCR. A detectability map can therefore be derived over the full range and Doppler detection space of the radar and denotes the minimum target RCS required for detection at each range and Doppler cell in an appropriate number of PRFs (often three). The detectability map may be thresholded at a given fixed RCS to indicate regions where a target of the given RCS would be visible/not visible. This thresholding forms the classic blind zone map for a medium PRF schedule. An example detectability map is given in Figure 5 based on a required detection SNCR = 0dB in at least three PRFs from a total of eight. Should a more realistic SNCR of, for example, +13dB be required for detection, one need only apply a 13dB offset to the detectability map data.

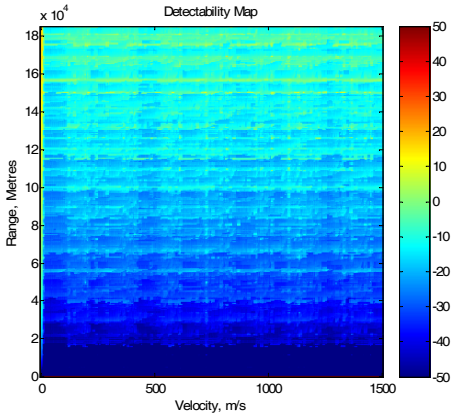

Figure 5: An example Detectability Map

Detectability maps are a useful means of characterizing relative performances in clutter. Each detectability map is valid given the assumptions made in the radar, antenna and clutter models and therefore comparisons between detectability maps are also valid. Furthermore, comparisons remain valid irrespective of any offsets which may be applied to the detectability maps (e.g. to set a detection criterion of SNCR ≥ +13dB) so long as a constant offset is applied to all detectability maps.

In many design applications it is necessary to compare two detectability maps in order to judge relative performances. Typically, a detectability map contains a total of around 10^5 to 10^6 range/velocity cells (pixels) and is stored as a two-dimensional array in which each element corresponds to a range/velocity cell. Since each pixel (element) refers to a consistent range/velocity cell, comparisons between two detectability maps can be made by comparing their matrix

elements. A number of comparison strategies may be formulated as in [4]. Here the authors describe two comparison metrics:

(i) The ratio of comparison

The "ratio of comparison" metric is derived on the basis of the ratio of the number of pixels in map *A* which exceeds those of map *B* to the number of pixels in map *B* which exceeds those of map *A*. This metric gives an impression of the relative area of the range/Doppler space for which the detectability of one test is greater than the detectability of another. However, this metric gives no information on the margin by which one is greater than the other.

(ii) The sum of difference.

The "sum of difference" metric is based on the sum of all the differences between the respective pixels of maps *A* and *B*. This metric gives an impression of the "aggregate" level by which the detectability of one test is greater than the detectability of another. However, one could not distinguish between the cases of a few elements in one matrix being significantly higher than those of the other matrix and most of the elements in one matrix being marginally higher than those of the other. Thus this metric indicates the margin of superiority but not its extent in area. The combination of the two metrics therefore indicates both the area extent of superiority of one detectability map over another and also on the aggregate margin of this superiority.

At low platform altitude (e.g. below 5000 metres) and look-down scenarios, target detection is clutter limited throughout most of the range/velocity detection space of the radar. At increasing altitudes and shallower grazing angles target detection becomes progressively more noise dominated. In a typical situation of an antenna depression angle of about 6^0 at a platform altitude of 11000 metres the detection space is largely noise limited, except in the region of MBC and any particularly high sidelobes. This has important implications on the design of the transmitted waveform (number of CPIs and FFT sizes) which results in the best use of the available beam dwell time for target detection. In noise limited cases, target detection is enhanced through the use of coherent integration of many pulses since the processing gain for targets is considerably higher than that for the noise. The signal to noise ratio (SNR) increases directly proportional to the FFT size. Hence large FFTs are favoured in noise limited cases. If the FFT size is large, each CPI time will be correspondingly long and there will not be the time for very many CPIs. However, when target detection is clutter limited, larger FFT sizes are not so beneficial since both targets and clutter are subject to similar processing gains. Some clutter decorrelation does occur on account of its ICM and does lead to signal to clutter ratio (SCR) improvements, however, the advantage is not so dramatic as for the noise limited case. In situations of high clutter it is better to use many different CPIs of differing PRFs since the exact range/velocity of high levels of clutter is PRF dependent. Thus over many PRFs one increases the likelihood that any given range/velocity cell becomes clear of high clutter levels in more PRFs. Most medium PRF schedules require target detection in at least three PRFs in order to resolve range and velocity ambiguities and so the aim is to ensure that each range/velocity cell is fairly clear of clutter in at least three PRFs. Therefore, increasing the number of PRFs (of correspondingly smaller FFT sizes) is advantageous in clutter limited scenarios. The generation of clutter maps enables the transition from noise limited to clutter limited cases to be judged.

4 Concluding Remarks

A method of modelling the surface clutter return for an airborne pulse Doppler radar has been described. The technique has been refined over several years in order to run efficiently and to faithfully model the real-world situation with integrity. The model is sufficiently flexible to permit additional functionality to be introduced, as desired. Similarly, several features are easily disabled if approximate results are required in a short time. This model has been applied in several research tasks, many of which have sought to optimise the selection of precise PRF values in medium PRF modes of operation [1]-[3][8] or to quantify the relative merits of difference antenna radiation patterns [4]. These models have proved useful in evaluating radar detection performance by deriving target detectability maps. In particular, they highlight regions of clutter limited detection versus noise limited detection. This is valuable when designing waveforms to make the best use of the available beam dwell time since noise limited detection is enhanced through the use of fewer CPIs of larger FFT sizes, whereas clutter limited detection favours the use of larger numbers of CPIs of smaller FFT sizes.

References

[1] C. M. Alabaster & E. J. Hughes. "The Design of Medium PRF Radar Schedules For Optimum Detectability in Diverse Clutter Scenes" *Proc. IEEE Waveform Diversity & Design*, Lihue, Kaua'i, HI, USA, 22nd – 27th Jan 2006.

[2] C. M. Alabaster & E.J. Hughes "Novel PRF Schedules for Medium PRF Radar", *Proc. Radar 2003*, Adelaide, 3rd - 5th Sept 2003.

[3] C. M. Alabaster, E.J. Hughes & J.H. Matthew. "Medium PRF radar PRF Selection Using Evolutionary Algorithms", *IEEE Trans. AES*, vol. 39, no. 3, pp. 990-1001, July 2003.

[4] C. M. Alabaster & E. J. Hughes. "The Dependence of Radar Target detectability on Array Weighting Function" *Proc. IEEE Radar 2007*, Edinburgh, 15th – 18th Oct 2007.

[5] M. M. Horst, F. B. Dyer and M. T. Tuley. "Radar sea-clutter model". URSI Dipest. 1978 Int. IEEE APiS URSI Sy.mp.., College Park, Maryland, USA

[6] "Radar Design Principles", Nathanson, 2nd Ed. Scitech Publishing Inc

[7] "Radar Handbook" Ed. M. Skolnik, 2nd Ed., McGraw-Hill

[8] D. A. Wiley, S. M. Parry, C.M. Alabaster and E. J. Hughes. "Performance Comparison of PRF Schedules for Medium PRF Radar", *IEEE Trans. Aerospace and Electronic Systems*. vol. 42, no. 2, Apr 2006, pp 601-611.